SN Computer Science (2024) 5:352
https://doi.org/10.1007/s42979-024-02742-3

ORIGINAL RESEARCH

Design of Chest Visual Based Image Reclamation Method Using Dual Tree Complex Wavelet Transform and Edge Preservation Smoothing Algorithm

B. P. Pradeep Kumar[1] · S. L. Shiva Darshan[2] · E. Naresh[3] · N. N. Srinidhi[4] · J. Shreyas[3]

Received: 27 May 2023 / Accepted: 19 February 2024

Abstract
The proposed article put forward a new scheme for image reclamation using second phase discrete symlet transform for medical images. The current medical image reclamation approaches have limitations in providing accurate reclamation fallouts with high visual insight and low computational complexity. To address these issues, this model presents a methodology for creating a medical image database using Image Reclamation using DT-CWT and EPS filter suited for the Resolution Enhancement of query chest image sample well utilized to get better retrieval rate where DWT algorithm is utilized for feature extraction of query input images. Flat and perpendicular prognoses of summation of pixels are analyzed to extract BC quantities, which are then used to compute the matching score of similarity for the images present in the database. The system selects the samples that are most pertinent to the given query sample image based on the matching score. The system's untrained database is used to obtain the photographs with the highest BC value. The projected method aims to improve the enhancement of sampled image by DT-CWT EPS algorithm to leads to increase the accuracy and efficiency of medical image reclamation for various research applications.

Keywords DWT · Healthcare systems · B quantities · Medical image · Visual BIR

Introduction

In the realm of modern healthcare, the retrieval of chest X-ray samples has emerged as a pivotal concern, necessitating advanced detection methods to meet the evolving needs of medical diagnostics. This imperative is driven by a motivation to revolutionize diagnostic accuracy and streamline medical imaging processes. As we navigate through the complexities of accurate chest sample diagnosis, the challenges inherent in this process underscore the indispensable role of machine learning and attention mechanisms. The significance of these challenges lies not only in their intrinsic complexity but also in the potential to significantly enhance the accuracy and efficiency of chest sample diagnosis.

In a typical Visual-Based Information Reclamation (VBIR) system, visual qualities, encompassing color, shape, texture, and spatial information, are automatically extracted from each image in the database based on pixel values.

This article is part of the topical collection "AI Based Internet of Healthcare: Analysis and Future Perspectives" guest edited by Diganta Sengupta, Debashis De and Prasenjit Bhadra.

✉ E. Naresh
naresh.e@manipal.edu

✉ N. N. Srinidhi
srinidhi.nn@manipal.edu

✉ J. Shreyas
shreyas.j@manipal.edu

B. P. Pradeep Kumar
pradi14cta@gmail.com

S. L. Shiva Darshan
shivadarshan@nitw.ac.in

[1] Department of ECE, HKBKCE, Bangalore 560045, Karnataka, India

[2] Department of Computer Science and Engineering, National Institute of Technology Warangal, Warangal 506004, India

[3] Department of Information Technology, Manipal Institute of Technology Bengaluru, Manipal Academy of Higher Education, Manipal, India

[4] Department of Computer Science and Engineering, Manipal Institute of Technology Bengaluru, Manipal Academy of Higher Education, Manipal, India

Published online: 27 March 2024

These extracted attributes are stored in a feature database, which is separate from the image database. Unlike the size of the picture data, the feature data for each visual aspect is considerably smaller. Within the feature database, each image in the image database is represented by a fixed-length real-valued multi-part feature vector or signature [1]. This vector encapsulates a condensed representation of visual attributes like color, texture, shape, and spatial information.

When a user initiates a query image through the VBIR method, the system, akin to its process for every image in the database, extracts the visual attributes of the query image. The subsequent step involves identifying images in the database whose feature vectors align with those of the query image [2]. These closest-matching images are then sorted based on their degree of similarity. VBIR outperforms text-based reclamation, operating with smaller, more efficient feature vectors rather than large-sized image data, thereby enhancing speed and effectiveness.

The utilization of a VBIR system can occur in two ways: firstly, for precise image matching, where a query image is compared with an image from the database to identify the most closely related photos. The second method involves approximate image matching, where the system identifies images that are most similar to a query image without requiring an exact match [3]. The block diagram of a semantic reclamation system, as illustrated in Fig. 1, visually encapsulates the structure and flow of this VBIR process.

Motivated by the imperative to innovate healthcare diagnostics, our study articulates clear research objectives aimed at developing a scalable digital image reclamation system. This system leverages the Visual-Based Image Reclamation (VBIR) method, specifically tailored to efficiently handle the nuanced complexities of large-scale histopathological digital images. To achieve this, our objectives include conducting a comprehensive literature review to assess the effectiveness of techniques mitigating X-ray segmentation issues within image VBIR. Additionally, the study proposes the implementation of discrete wavelet transform to quantify image characteristics, determining the Flat, perpendicular summation, and prognosis of the images. Furthermore, we aim to leverage the Bhattacharyya coefficient for the retrieval of similar images in the VBIR method. These objectives collectively define a unique and comprehensive framework, aligning with the broader motivation to advance diagnostic capabilities.

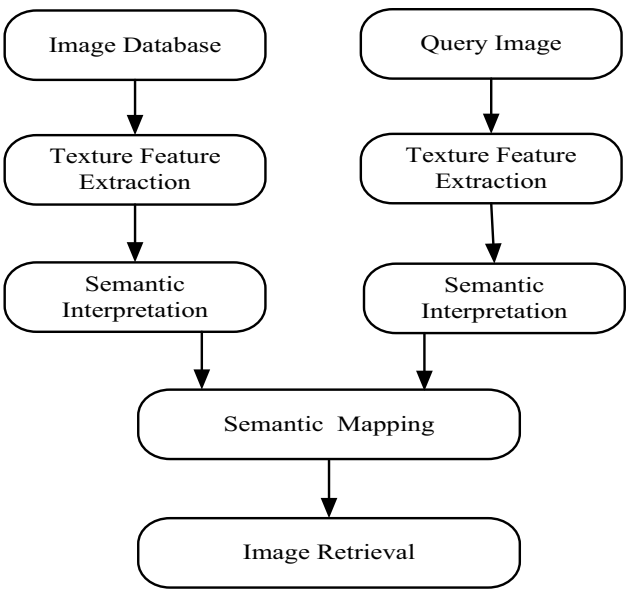

Fig. 1 Block diagram of semantic reclamation system

Within the dynamic realm of Visual-Based Information Reclamation (VBIR), the challenge transcends the retrieval of well-defined images, extending to the complexities of chest X-ray images in vast, heterogeneous databases. This dynamic and flexible field presents challenges that vary based on the area of interest, database size, and the availability of prior knowledge. At one end of the spectrum, retrieving images with clear context, such as logos based on distinctive shape traits, is relatively straightforward. However, at the other end, the task of extracting meaningful chest X-ray images from enormous collections, akin to those on the World Wide Web, introduces a formidable challenge.

Central to the problem in VBIR is the disparity between low-level visual elements used by computers for image indexing and the high-level semantic ideas employed by humans for image comprehension. This research aims to contribute to the resolution of these challenges, specifically within the context of chest X-ray sample retrieval, motivated by the broader vision to propel healthcare diagnostics into a realm of enhanced accuracy and efficiency.

Table 1 provides a concise summary of various techniques employed in the taxonomy of chest X-ray image retrieval. Each technique is described along with its applications, pros, and cons, offering insights into their diverse functionalities and considerations for implementation in medical imaging.

Recognizing the need for a more advanced and efficient approach, contemporary visual-based image retrieval (VBIR) systems have shifted towards storing and retrieving visual information based on the inherent properties of images. The elements such as color, form, texture, and spatial arrangement play a central role in the VBIR approach, wherein the visual features of images in a database are extracted and represented as multi-dimensional feature vectors. These vectors are then stored in a feature database, forming the foundation for an effective and precise VBIR system [4].

In the image reclamation process, users submit sample photos or sketches, which the system transforms into internal feature vector representations. The system subsequently assesses the dissimilarity between the feature vectors of the

Table 1 Overview of chest X-ray image retrieval techniques

Technique	Description	Application	Pros	Cons
Content-based retrieval	Utilizes image content features, including shape, texture, and intensity, to retrieve similar chest X-ray images from large databases	Content-based image retrieval, similarity matching	No need for annotations, useful for large datasets	Sensitivity to variations in image quality, limited semantic understanding
Semantic segmentation	Focuses on segmenting different anatomical structures within chest X-ray images, aiding in the precise localization of abnormalities	Organ segmentation, abnormality localization	Detailed anatomical understanding, precise localization	Sensitive to image noise, requires annotated data
Wavelet transform	Applies discrete wavelet transform to analyze frequency components of chest X-ray images, facilitating feature extraction and representation	Multiresolution analysis, feature extraction	Captures both global and local features	Sensitivity to noise, selection of appropriate wavelet basis
Bhattacharyya coefficient	Measures statistical similarity between probability distributions, allowing for efficient retrieval of chest X-ray images based on their visual characteristics	Similarity-based retrieval, content matching	Robust to variations in image appearance	Limited expressiveness for complex visual patterns
Ensemble methods	Combines multiple retrieval techniques or models to enhance overall performance and robustness in chest X-ray image retrieval scenarios	Improved accuracy, increased robustness	Mitigates individual model weaknesses	Increased computational complexity, potential redundance

query sample or sketch and those of the images in the database. The retrieval procedure employs an indexing strategy to facilitate swift searches within the image library.

Effective indexing and rapid image reclamation, particularly based on optical attributes, pose critical challenges in visual-based image reclamation. Given the high dimensionality of feature vectors in sampled data, conventional indexing structures become unsuitable. Consequently, dimensionality reduction techniques, such as Principal Component Analysis (PCA), are often employed to establish an effective indexing scheme. PCA maps the data onto a subspace, redirecting concentrated variation in the data.

Novelty: The study introduces a novel approach for chest visual-based image reclamation, utilizing the Dual Tree Complex Wavelet Transform (DTCWT) in tandem with an Edge Preservation Smoothing Algorithm. This fusion of techniques addresses existing challenges in enhancing chest X-ray images under limited resources or suboptimal imaging conditions. The novelty of the study lies in several key aspects. Firstly, the integration of DTCWT offers improved directional selectivity and shift invariance, enabling accurate feature extraction and reconstruction of fine details and textures present in chest X-ray images. Secondly, the proposed Edge Preservation Smoothing Algorithm intelligently preserves edges while reducing noise and artifacts, striking a balance between image clarity and detail preservation. This algorithm significantly contributes to the overall efficacy of the image reclamation method by mitigating the risk of over-smoothing, a common issue in traditional enhancement techniques. Thirdly, the study focuses specifically on chest X-ray imaging, addressing the unique challenges associated with this modality, such as low contrast, noise, and subtle anatomical structures.

The system architecture of image reclamation, as illustrated in Fig. 2, emphasizes the reliance of the Visual-Based Image Reclamation System (VBIR) on the visual characteristics of images for extracting informative features. Evolving from VBIR, Image Mining techniques further advance the extraction of visual aspects, including color, texture, pattern, image topology, object shape and layout, and their locations within the image. The system leverages various features, such as color information, texture analysis, contour detection (shape), image topology, background pattern, and object location, to execute image reclamation effectively [2].

This research paper significantly advances the field of medical image processing and analysis through the following notable contributions:

- Integration of Leading-Edge Techniques: The paper introduces the integration of DT-CWT and EPS algorithms, effectively enhancing the quality of chest images.
- Robust Quantitative Evaluation: Robustly evaluates image quality improvement using statistical parameters, providing an objective assessment of the proposed methodology.
- Feature analysis: Enhances image retrieval capabilities by leveraging Bhattacharyya Coefficients and 2D-DWT, streamlining access to pertinent medical images.
- Impressive Experimental Results: The paper conducts extensive experiments on a dataset comprising 26 chest X-ray samples. The achieved high PSNR, low RMSE, and minimal entropy underscore the effectiveness of the proposed approach.
- Retrieval Score Enhancement: Demonstrates an increase in the retrieval score for the top ten matching images,

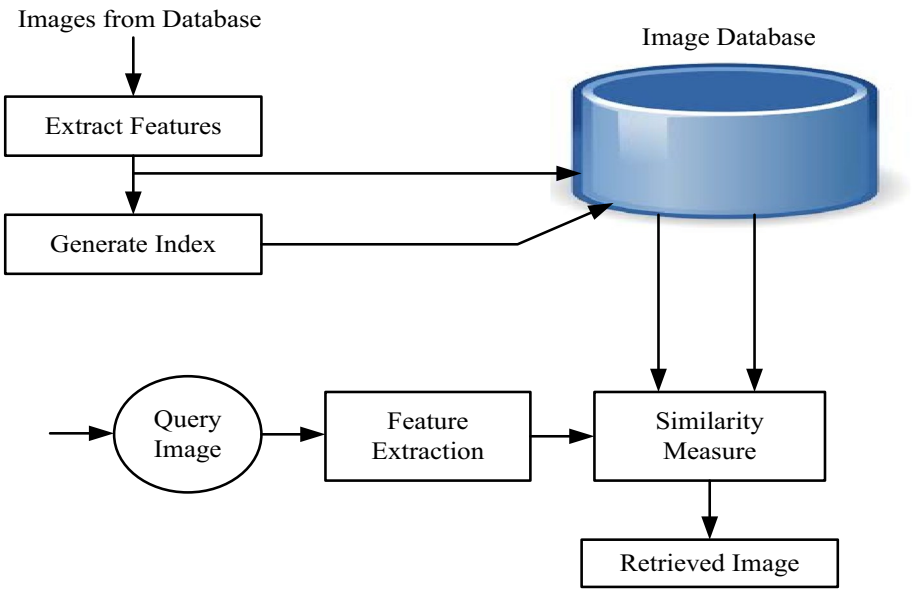

Fig. 2 System architecture of image reclamation

emphasizing the practical utility of the proposed method in medical image analysis and diagnosis.

Our research article is meticulously structured to guide readers seamlessly through a coherent journey. "Review of literature" initiates with an in-depth exploration of the existing literature, delving into image reclamation techniques and their real-world applications within the realm of chest visuals. Serving as the gateway to our innovative approach, "Proposed system design" introduces "proposed Algorithm." This section lays the groundwork for our research, elucidating key concepts and methodologies. In "Results", we present empirical results derived from experiments, substantiated through both visual comparisons and quantitative assessments, validating the efficacy and practicality of our framework. "Conclusion" acts as a pivotal juncture, encapsulating primary research findings and providing valuable insights while also unveiling potential future research directions in this dynamic field.

Review of Literature

In their research, Zhongwei et al. [5] developed a method for appreciation and reclamation of noisy and incomplete shoeprints datasets by extracting key feature points and performing similarity matching. The research discovered that among all shoeprints, full-measure prints and toe prints had the best performance. Additionally, the proposed system was able to effectively handle noise in the images with minimal modification in appraisal between original and raucous shoeprints.

Mohanapriya et al. [6] proposed a robust reclamation system using a supervised classifier that focuses on isolated features. Grain topographies were mined using the gray level co-occurrence environment algorithm, and feature optimization was performed to select the best features for training the classifier. The dataset was classified into three classes: normal, benign, and malignant, and the query image was classified to a specific class to retrieve relevant images from the database. The study also aimed to improve accuracy by calculating precision and recall values and storing images at different feature extraction stages in the database.

Ghosh et al. [7, 8] planned a design detect the presence of malaria by identifying chromatin specks within red blood cells (RBCs). The algorithm utilized 4-connected labeled region maps to analyze and manipulate the image by removing unwanted artifacts and counting RBCs. Alternative methods for detecting chromatin spots within the RBCs were also presented, and the accuracy and recall efficiency of the algorithm were evaluated.

To acquire the best possible quantized image in the cloud, Muppidi et al. [1] have suggested a flexible and affordable architecture for parallelizing container-based quantization algorithms. Large datasets can be used with this strategy because it is scalable. In this study, fuzzy entropy and evolutionary algorithm-based techniques are used as quantization methods. To calculate the fuzzy entropy, various membership functions are used by each procedure. The Structural Similarity Index (SSIM) is used to select the best quantized image. This strategy is a cutting-edge way for efficiently and concurrently resolving time-consuming and tiresome serial problems. The results are consequently noticeably superior to those attained using a serial technique.

The Wordometer, a novel method for counting the words a user reads, was developed by Kunze et al. [2] utilizing a mobile eye tracker and document image reclamation. Using tenfold cross-validation, we have created a reading detection system that can quantify reading with over 91% accuracy across ten test individuals. Two algorithms that assess read words using a line break identifier have been put into place. The more sophisticated word count approach, based on support vector regression with an RBF kernel, produces an average mistake rate of just 8.2% (6.5% if one subject with anomalous behavior is eliminated), as opposed to the simpler algorithm's average error rate of 13.5% for nine users over ten documents. These inaccuracy rates are similar to the step counts that pedometer, which track our daily steps, produce. Therefore, we think that the Wordometer can be utilized as a "step counter" for the knowledge we read, enhancing the efficiency of our learning.

An efficient and quick object matching operation is combined with a local descriptor that is derived from the accelerated robust feature algorithm in Cedillo et al.'s [3] fast visual-based video reclamation system. Compressed video data are partially decoded to produce discrete cosine transform quantities of key frames, which are then used to obtain sub-block quantities and a down-sampled version of edges. The preliminary results are ranked using an efficient colour descriptor based on the colour correlogram and dominant colour descriptors.

Accuracy and recall metrics are used to gauge how well the suggested technique is working. The experimental outcomes demonstrate the efficacy of the suggested method when used on a collection of videos documenting Mexican Cultural Heritage.

SenGupta et al. [9] contend that it is crucial to concentrate on the point of interest rather than accessing the complete video because of the enormous growth in multimedia and technology. Utilizing visual-based video reclamation, the interest areas are efficiently indexed and retrieved. Shot boundary detection is the first stage in CBVR. For simple indexing and video recovery, the video must be divided into shots. Therefore, segmentation is crucial to the processing of digital media, pattern identification, and computer vision. We discuss various methods for solving the shot boundary detection issue in this paper [10].

Table 2 provides a comparative overview of diverse image reclamation techniques employed in relevant studies. Each technique is evaluated based on its application domain, main focus, key findings, and its relevance to the proposed research paper. the comparison highlights the diverse applications and emphases of each technique. While Zhongwei et al. focus on shoeprints, Mohanapriya et al. concentrate on medical images, Ghosh et al. on malaria detection, Muppidi et al. on cloud-based quantization, Kunze et al. on document image reclamation, Cedillo et al. on visual-based video reclamation, and SenGupta et al. on focusing on points of interest in videos. Each study brings unique contributions to its respective domain, providing valuable insights and methodologies.

Table 2 Comparative analysis of image reclamation techniques

Aspect/technique	Zhongwei et al. [5]	Mohanapriya et al. [6]	Ghosh et al. [7, 8]	Muppidi et al. [1]	Kunze et al. [2]	Cedillo et al. [3]	SenGupta et al. [9]
Application domain	Shoeprints datasets	Medical Imaging	Malaria detection in RBCs	Cloud-based quantization	Document image reclamation	Visual-based video reclamation	Visual-based video reclamation
Main focus	Appreciation and reclamation of shoeprints	Robust reclamation system for medical images	Malaria detection through chromatin specks in RBCs	Scalable quantization architecture	Word counting through eye tracking	Efficient object matching and local descriptors	Focusing on points of interest in videos
Key findings	Full-measure prints and toe prints performed best	Effective classification into normal, benign, malignant	Efficient removal of unwanted artifacts and counting RBCs	Fuzzy entropy and evolutionary algorithms	Unique method for counting words	Fast video retrieval with color correlogram descriptor	Efficient indexing and retrieval of interest areas
Relevance to research paper	Feature extraction and similarity matching	Robust feature extraction and classification	Precise detection in medical images	Innovative quantization in the cloud	Advanced document image analysis	Efficient video reclamation with object matching	Precise indexing and retrieval of interest areas
Common theme/emphasis	Feature extraction and similarity matching	Robust feature extraction and classification	Precise detection in medical images	Scalable and efficient quantization methods	Unique methods for document image analysis	Efficient video reclamation with object matching	Precise indexing and retrieval of interest areas

Proposed System Design

The following passage describes the required system architecture for creating an adaptable digital image reclamation system utilizing VBIR techniques to effectively manage large-scale MRI digital images. Matlab v.2015 (a) is the chosen software tool for implementing this framework.

System Architecture

In Fig. 3 the proposed technique for a computerized medical chest image division framework for X-ray images is presented. The model comprises of three main junctures. Firstly, a VBIR approach is used to recognize a small set of medical chest image CXR sample images that are most alike to the patient's samples X-ray [11, 12]. This is accomplished through B-coefficients i.e., similarity match measure by the use of partial Radon transforms. Similarity Matched high score chest images retrieved by this method match the patient's chest well and efficiently create an anatomical map using medical VBIR methods. The DT-CWT technique employs Lanczos interpolation to further enhance edge detection and linear feature identification. This process involves mapping each input image pixel to a translated and scaled copy of the Lanczos kernel.

$$L(x) = \begin{cases} 1 & \text{if } x = 0 \\ a * \sin(\pi x) * \sin(\pi x/a)/(\pi x)^2 & \text{if } 0 < |x| \; a \\ 0 & \text{otherwise} \end{cases} \quad (1)$$

The EPS technique is applied. EPS leverages a Gaussian low-pass filter to preserve essential image features, particularly edges while reducing noise. The mathematical representation of $EPS(I(x, y)) = I(x, y) * G\sigma(x, y)$, where $G\sigma(x,y)$ is the 2D Gaussian kernel with standard deviation σ.The next step is to create an anatomically guided patient-specific

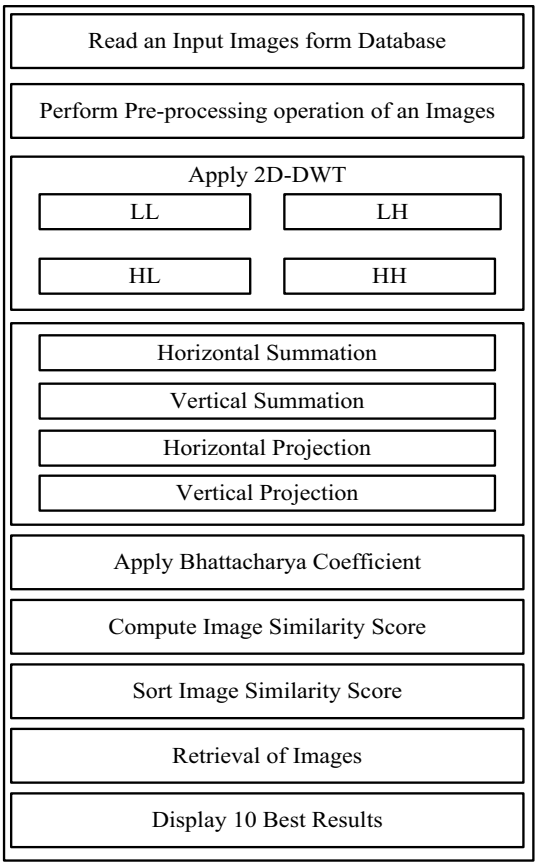

Fig. 3 Proposed system design of the model

chest model by using a cutting-edge deformable registration algorithm to deform the X-rays in the training library to fit the patient's X-ray. several statistical quality parameters are employed to assess the quality of the enhanced image.

The entropy H of an image I(x, y) is a measure of the amount of information or uncertainty in the image's pixel values and is computed as shown in the Eq. 2:

$$H(I) = -\sum_{x,y} p(I(x,y)) \cdot \log_2(p(I(x,y))) \tag{2}$$

where, p(I(x, y)) is the probability distribution of pixel values in the image. SSIM is a measure of the structural similarity between two images and can be explained as shown in the Eq. 3

$$SSIM(I1, I2) = \frac{(2 \cdot \mu 1 \cdot \mu 2 + C1) \cdot (2 \cdot \sigma 12 + C2)}{\left(\mu_1^2 1 + \mu_2^2 2 + C1\right) \cdot \left(\sigma_1^2 + \sigma_2^2 + C2\right)} \tag{3}$$

where, μ1 and μ2 are the means of the two images, σ21 and σ22 are their variances, σ12 is their covariance, and C1 and C2 are constants to stabilize the division.

$$PSNR = 10 \cdot \log_{10}\left(255^2/MSE\right) \tag{4}$$

where 255 is the maximum pixel value (for an 8-bit image) and MSE = 1/N∑Ni = 1(I(i) − I^(i))2 is the mean squared error, and N is the total number of pixels. RMSE = $\sqrt{}$ MSE measures the average magnitude of the differences between corresponding pixel values in the original image I and the processed image I^. contribute to image enhancement, followed by the analysis of statistical quality parameters.

The chest limits are then established using a discrete graph cut optimization method with a unique energy function. The energy function has a unique anatomical map shape prior term that makes sure the chest anatomy is adhered to precisely. To develop a patient-specific chest model, a collection of best fit training maps is chosen from the anatomical database of fragmented chest images. When a patient's X-ray and pre-segmented chest images from the CXR database are compared using a quick shape similarity metric based on partial Radon transforms, the registration performance is greatly enhanced [13].

The training data for the SVM consists of sockets (vectors) xi, each associated with a category yi. In a given aspect d, Xi € Rd, and Yi takes values of either + 1 or − 1. The equation is defined as <W·x + b> = 0, where W € Rd, <W, x> denotes the interior dot product, and b is a real constant.

The image projection, denoted as H1 and H2, play a crucial role in classifying. Specifically:

$$H1: W \cdot x + b = +1 \tag{5}$$

$$H2: W \cdot x + b = -1 \tag{6}$$

These projections and summation process are designed to effectively separate regions in the image. When Yi = + 1, the state is W·x + b ≤ − 1 for H1, and when Yi = − 1, the state is W·x + b ≥ + 1 for H2. This distinction aids in accurately classifying the chest samples.

Data Flow Diagram

DFD is a visual approach to illustrate the system's process flow. During the initial and analysis stage, a model is used to represent how data is processed and moves through the system. The models consist of core processes, data stores, and data flows between various models. This technique is employed to demonstrate how data will pass through a series of processing levels or steps [14].

Level Zero Data Flow Diagram

Figure 4 depicts a Level-0 Data Flow Diagram that illustrates the primary process involved in the chest segmentation

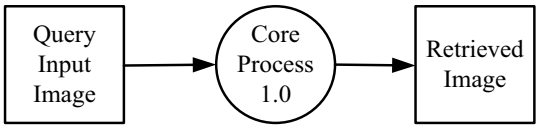

Fig. 4 Level-0 DFD

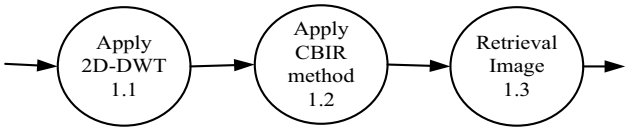

Fig. 5 Level-1 DFD

method {1}. This process takes a query histopathological chest image and utilizes Visual-based image reclamation technique to process it into the resulting retrieved image.

The Level-1 Data Flow Diagram, as illustrated in Fig. 5, is a detailed breakdown of the Level-0 DFD. It reveals that the primary process {1} is now succeeded by three subprocesses: 2D-DWT process {1.1}, the application of VBIR method {1.2}, and the reclamation of the resulting image {1.3} [15].

Figure 6 illustrates Level-2 DFD is presented, which represents the breakdown of the 2D-DWT technique {1.1}. This process involves the computation of approximation quantities, such as LL coefficient elements {1.1.1}, from digitized histopathological images. Additionally, the remaining detail quantities, including LH, HL, and HH quantities, are computed and stored in vectors {1.1.2}. Furthermore, the Flat summation, perpendicular summation, Flat prognose, and perpendicular prognose are generated at this stage and will be displayed {1.1.3}.

Figure 7 displays the Level-2 Data Flow Diagram, which is a detailed version of the VBIR process. During the VBIR process, robust features with multi dimension are identified from the probe image and projected onto binary codes. The image training {1.2.1} can then be conducted. Following the training stage, the Bhattacharyya coefficient algorithm {1.2.2} is applied to establish the similarity score for each sample in the catalogue. Finally, the sample data similarity score for each image is calculated.

In Fig. 8, the Level-2 Data Flow Diagram illustrates the breakdown of the Reclamation of Image {1.3} process. This process is decomposed into three subprocesses: sorting image similarity scores {1.3.1}, displaying the top 10 matching images {1.3.2}, and retrieving images based on the best similarity scores and Bhattacharyya score {1.3.3}. These steps are necessary to perform reclamation of biomedical images [16].

Fig. 6 Level-2 DFD

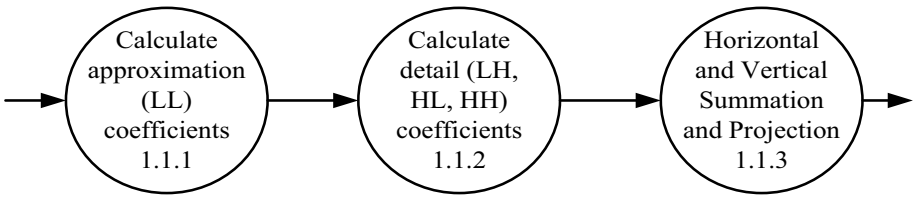

Fig. 7 Level-2 DFD

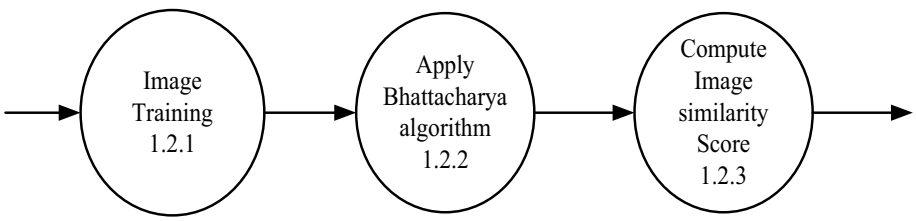

Fig. 8 Level-2 DFD

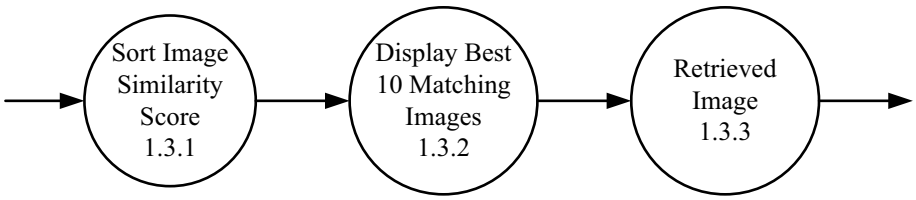

Pseudo Code for Training of Reclamation System

```
Start
Input I, bins2, H2, bibs1, H1, Sc, Sr;
Load database;
Take query image;
For (  i=size of database) then
 H10← database (1);
Bins10← database (2);
H20← database (3);
Bins20← database (4);
Itemp← database (5);
Sr0← Accomplish outline row wise;
Sc0← Accomplish outline column wise;
Calculate Bhattacharyya quantities;
P← find out unique binse;
Generate respective bins;
 q ← intersect (bins2, bins20);
 n ← length(p);
 m ←length(q);
 Alpha ← n/(n + m);
 p-temp ← 0;
p-temp ←  ptemp + sqt(p1(x)*p2(x));
q-temp ← q-temp + sqt(q1(y)*q2(y));
  BC ← alpha*p-temp + (1-Alpha)*q-temp;
  BCi(ii) ← round(BC);
  Display (database image score);
 Display ('Bhattacharya score');
End;
Find top 5 matching images;
Stop;
```

The following is a explanation of the given code: Begin by providing input parameters, including I, bins2, H2, bibs1, H1, Sc, and Sr. Next, load the database and select the enquiry samples. For each samples in the database (i.e., for i in the size of the database), retrieve the values of H10, Bins10, H20, Bins20, and Itemp from the database. Calculate Sr0 and Sc0 by performing summation operations row-wise and column-wise, respectively. Compute the Bhattacharyya quantities and determine the unique bins (p). Generate the respective bins and perform an intersection with bins20 (q). Calculate the length of p (n) and q (m) and compute alpha as n/(n + m). Next, calculate ptemp and qtemp by taking the square root of p1(x)*p2(x) and q1(y)q2(y), respectively. Compute the Bhattacharyya score (BC) as alphaptemp + (1-alpha)*qtemp and round it to obtain BCi(ii). Display the database image score and Bhattacharyya score. After completing the loop for all images in the database, find the top 10 matching images and stop [17].

Bhattacharyya Quantities

In the Image Projection and Summation process, the image projection (H1, H2) and projection bins1 and bins2 are crucial for article extraction and resemblance shrewdness. The summation along commotions Sr0 and poles Sc0 of the catalogue samples Itemp is figured to originate meaningful configuration illustrations. The summation progression improves the capability to seizure relevant shapes and appearances for assessment. The crossing procedure has a pivotal role in recognizing the appearances between the chest query sample and the catalogue images, assisting in the reclamation of pertinent metaphors. To obtain the juncture (Q) of binsN1 and binsN2, which relates to the collective essentials among the two sets given by the Eq. 7.

$$Q = \text{binsN1} \cap \text{binsN2} \tag{7}$$

where Q signifies the set of collective structures. This complementary step foils any one article from dominating the alike shrewdness and augments the robustness of the system. the Bhattacharyya quantity (BQ) is a arithmetical ration used to enumerate the likeness between two likelihood disseminations given by Eq. 8

$$BQ = Xni = 1pP(i) \cdot Q(i) \tag{8}$$

where n represents number of distinctive bins in the disseminations. The procedure involves discover the top 10 matching images from the catalogue based on the uppermost Bhattacharyya quantities (BQi). This is achieved by calculating statistical parameters of a channel,.This is achieved using the following Eq. 9 In the context of image reclamation, the BQ is employed to assess the resemblance between the article vectors of the probe sample and the images stored in the catalogue. It serves as a critical resemblance measure for image reclamation, ensuring accurate matches for the given probe sample.

This is accomplished through the application of Eq. 9. In the realm of image retrieval, the Bhattacharyya quantities (BQ) is utilized to evaluate the similarity between the article vectors of the probe sample and those of the images archived in the catalogue. It stands as a pivotal metric for gauging resemblance in image retrieval, guaranteeing precise matches for the provided probe sample.

$$\text{Uppermost 10 Identical Metaphors} = X(BQi) \tag{9}$$

The function argmaxi is utilized to identify the indices corresponding to the highest 10 values of BQi. These indices point to the top-matching images, signifying optimal outcomes for the probe sample. This information proves invaluable in medical diagnosis and research contexts, offering significant insights. The presented pseudo-code outlines the procedural steps for training the reclamation system.

Figure 9 depicts the process flow chart of the proposed technique. The automated chest image is taken as input and its image features are extracted. Medical imaging segmentation presents several challenges such as AWGN, occlusion during capturing, scanning articles, low contrast, tissue distortion. Traditional dissection methods that make streamlining conventions of rigid motion and will not have prior evidence usually yield unacceptable results on biomedical datasets. We integrate a chest atlas model into the system to provide previous knowledge for better segmentation. Since chest shapes can vary in X-ray pictures, The chest areas cannot be adequately described by a static model. In order to determine a statistical model for each patient's X-ray, our system first identifies the most similar images from a training set of segmented images (atlases), then uses a non-rigid registration algorithm to deform those training atlases into the patient CXR [18].

Here's a Algorithm of retrieval system of the pseudo code:

1. Begin Reclamation of Image:
2. Input query image (I), image histograms (H1, H2), and histogram bins (bins1, bins2), similarity score (Sc), and row-wise sum (Sr).
3. Load database images.
4. For each image in the database: a. Retrieve histogram and bin values (H10, Bins10, H20, Bins20). b. Retrieve image ID (Itemp). c. Compute row-wise sum (Sr0) and column-wise sum (Sc0). d. Calculate Bhattacharyya quantities. e. Determine unique bins (P) and generate respective bins. f. Compute intersection of bins (q). g. Calculate alpha value. h. Calculate ptemp and qtemp values. i. Compute Bhattacharyya coefficient (BC) and round it to nearest integer (BCi). j. Display image score and Bhattacharyya score.
5. End loop.
6. Find top 5 matching images based on highest Bhattacharyya scores.
7. End Reclamation of Image.

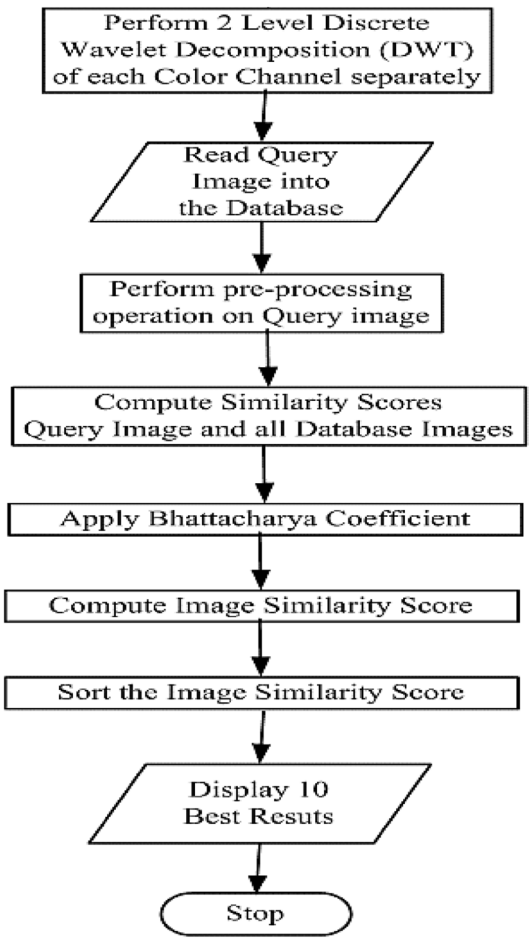

Fig. 9 Process flow chart of the proposed technique

Results

The results obtained for VBIR techniques, in this proposed robust segmenting model for classifying the region of interest in radiological images of chest. It comprises the assemblage of Chest radiological images has been preserved into the catalogue folder. The organization of the dataset is mainly characterized by the feature set of collected samples. This part explains the matlab platform usage with identification of similar pattern and reclamation methods (Fig. 10).

Table 3 offers a comprehensive comparison of various image interpolation algorithms, evaluating their performance across critical metrics. Notably, the Nearest algorithm exhibits the lowest PSNR at 26.24 dB, indicating a reduction in image quality. Additionally, it registers the highest RMSE at 12.37, highlighting a larger average discrepancy between predicted and actual values. The SSIM

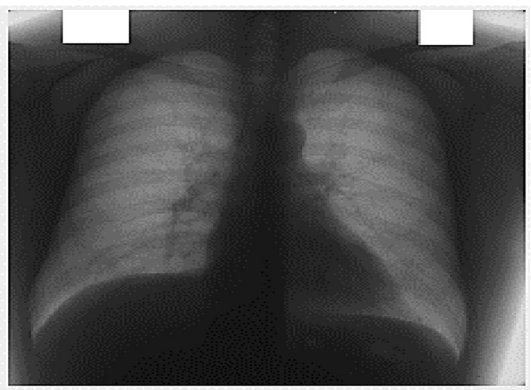

Fig. 10 Input query image A

Table 3 resolution enhancement algorithms for input query image A

Algorithms	PSNR	RMSE	Entropy	SSIM
Nearest	26.24	12.37	4.46	0.91
Bilinear	28.08	10.01	4.70	0.94
Bicubic	28.11	10.11	4.88	0.92
DT-CWT	28.50	13.8	0.031	0.93
DT-CWT and EPS	29.07	10.006	4.81	0.95

of 0.91 further underscores its comparatively diminished capability in preserving structural information. Bilinear and Bicubic methods show incremental improvements over Nearest, particularly with Bilinear achieving the lowest RMSE at 10.01. While the Discrete Transform Continuous Wavelet Transform (DT-CWT) algorithm demonstrates commendable PSNR (28.50 dB) and a respectable SSIM of 0.93, its higher RMSE at 13.8 suggests a compromise in accuracy. The DT-CWT and EPS algorithm, although not securing the absolute best results, stands out with a PSNR of 29.07 dB, RMSE of 10.006, and SSIM of 0.95. These scores, while not the pinnacle in each category, collectively position it as a robust performer, demonstrating a balanced trade-off between accuracy and structural preservation. It is essential to note that, despite not clinching the top spot in every metric, the DT-CWT and EPS algorithm emerges as a comparably strong contender, showcasing versatility and proficiency across multiple evaluation criteria. The Entropy metric further delineates nuances in image characteristics, with Nearest having the highest entropy (4.46) and DT-CWT having the lowest (0.031). In summary, the DT-CWT and EPS algorithm emerges as a well-rounded performer, offering competitive results across a spectrum of metrics.

Figure 11 gives overall comparative graph of the all the samples i.e., 26 images and showing the significant representation. The figure presents a comprehensive evaluation of various entities labeled from A to Z, each representing a distinct image or condition, based on key image processing metrics. Peak Signal-to-Noise Ratio (PSNR), which measures image quality, reveals that Entity I boasts the highest PSNR at 30.77, indicating superior image quality, while Entity Z records the lowest at 26.72. Root Mean Square Error (RMSE), reflecting the accuracy of predictions, highlights Entity P with the lowest RMSE at 7.85, signifying minimal average prediction errors, while Entity Z exhibits the highest at 14.6. The metric of Entropy, which gauges image randomness, shows that Entities C and R have the lowest entropy values at 0.01 and 0, respectively, implying a more ordered image structure. Conversely, Entities V, W, X, Y, and Z display higher entropy values, indicating increased randomness. Structural Similarity Index (SSIM), quantifying the similarity between images, underscores Entity F with the highest SSIM at 0.96, reflecting excellent preservation of structural information. Conversely, Entities W and X demonstrate the lowest SSIM values at 0.81 and 0.87, respectively, suggesting challenges in maintaining structural similarity. In summary, Entity I emerges as a top performer across metrics, while Entities F, O, P, and U also exhibit commendable overall performance. Entities W, X, Y, and Z, on the other hand, face difficulties in preserving structural information, as indicated by lower SSIM values.

In Fig. 12, we present a detailed comparative graph encapsulating the parametric values of PSNR, RMSE, Entropy, and SSIM for all 26 sample images subjected to the DT-CWT and EPS conditions. Each sample, denoted from A to Z, is distinctly marked on the graph, providing a visual representation of the algorithm's performance across the entire dataset. The graph enumerates the variations in PSNR, offering insights into the signal-to-noise ratio and highlighting samples with superior image fidelity. Additionally, the fluctuations in RMSE values are visually depicted, aiding in the identification of samples with closer alignment to the original images. The distribution of entropy values is represented, offering a glimpse into the randomness of visual content across the dataset.

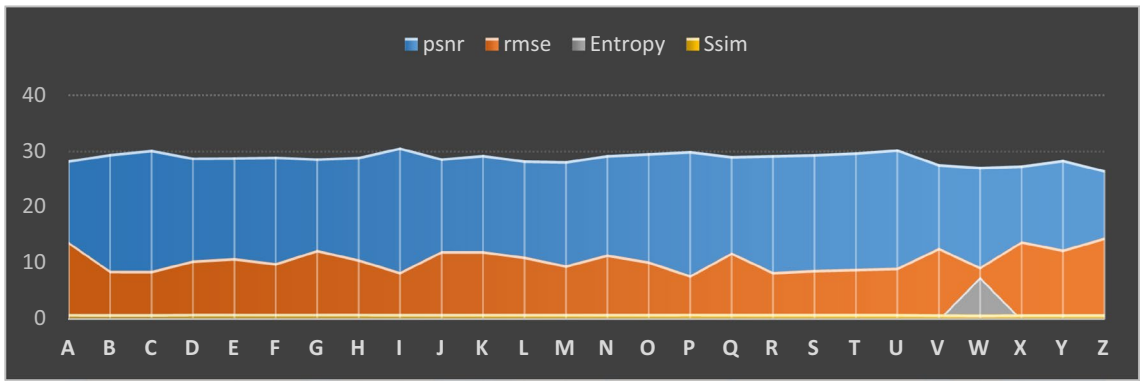

Fig. 11 Illustration of PSNR, RMSE, entropy, SSIM values for the algorithm DT-CWT

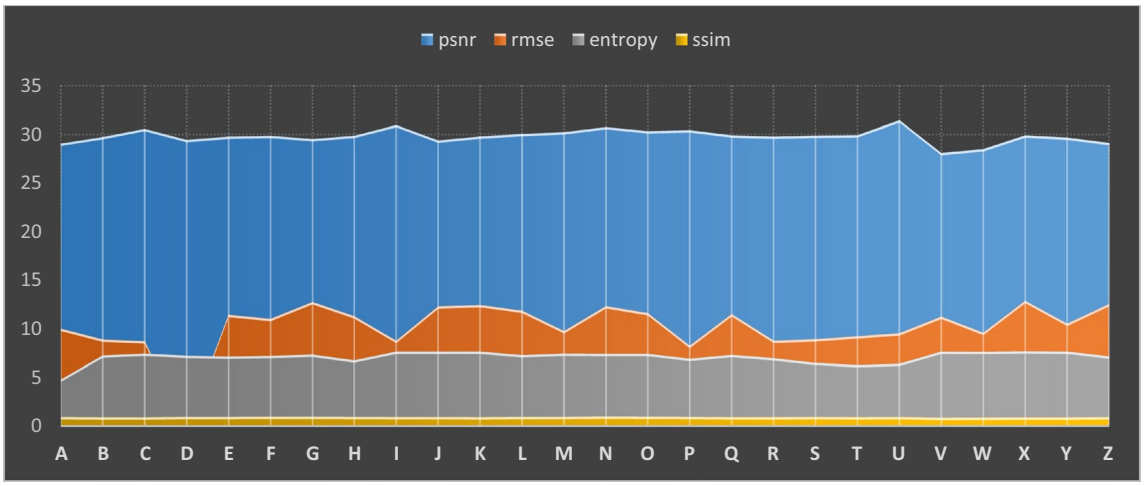

Fig. 12 Illustration of PSNR, RMSE, entropy, SSIM values for the algorithm DT-CWT and EPS

Furthermore, the graph illustrates the trends in SSIM values, emphasizing structural similarity patterns among the samples. Peaks and troughs in the graph serve as indicators of notable performance metrics, and any discernible clusters or patterns may suggest similarities or differences among specific groups of samples.

Multi Scale Decomposition will lead to robust feature sets collection that points towards Edge Preservation Smoothing to Resolution Enhancement of sampled data. In order to create the enhanced image, the proposed DT-CWT and EPS algorithm images are divided into several sub bands, interpolated, and then the sub bands are reconstructed.

The input image is first performed decomposition using the wavelet transformation method. The wavelet transformation will be performed with respect to discrete and continuous wavelet transform; the level of decomposition is also specified during the process. In the DWT the source function cast-off 'symlet' mama wavelet. After the application of DWT in to the image, the image is decomposed into two parts, the estimate quantities and the meticulous quantities. The approximation quantities are taken into the consideration. Similar procedure is applied to CWT. The obtained decomposed approximation quantities are sent to interpolation block for further processing.

Figure 13 showcases a meticulously designed Graphical User Interface (GUI) that has been carefully tailored to optimize the execution of the Discrete Wavelet Transform (DWT) operation, specifically utilizing Haar wavelets, on the designated query image. This interface is intricately crafted to empower users in the seamless extraction of crucial image coefficients through the DWT process.

Moving forward, Figs. 14, 15, 16, and 17 provide a visual representation of the outcomes yielded by the Discrete Wavelet Transform operation. These figures unveil the resulting sub-band coefficients, namely LL (Low–Low), LH (Low–High), HL (High–Low), and HH (High–High). Each of these sub-bands serves a distinct purpose in characterizing various aspects of the image. The LL sub-band encapsulates the approximate image, capturing low-frequency components and offering a comprehensive overview of the image's structural elements. Simultaneously, the LH sub-band excels in extracting horizontal features, shedding light on details associated with changes in intensity or color along the image's horizontal axis. Conversely, the HL sub-band directs its focus towards vertical features, accentuating variations along the vertical axis. Lastly, the HH sub-band isolates diagonal features, highlighting patterns or structures that diagonal orientations within the image may unveil.

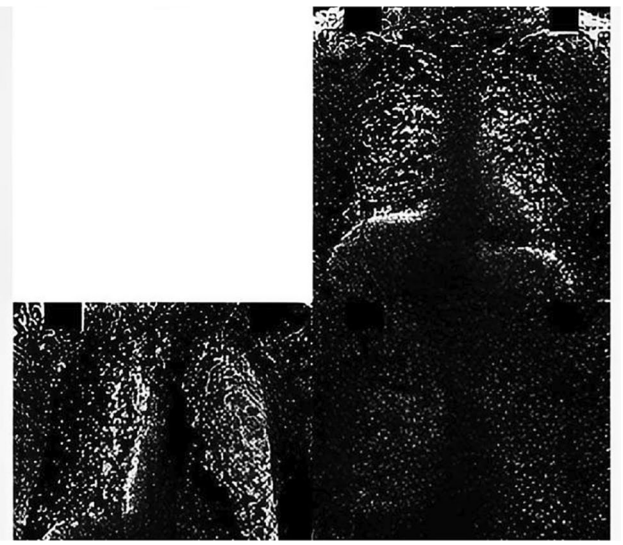

Fig. 13 DWT quantities profile of input query image: insights into frequency components

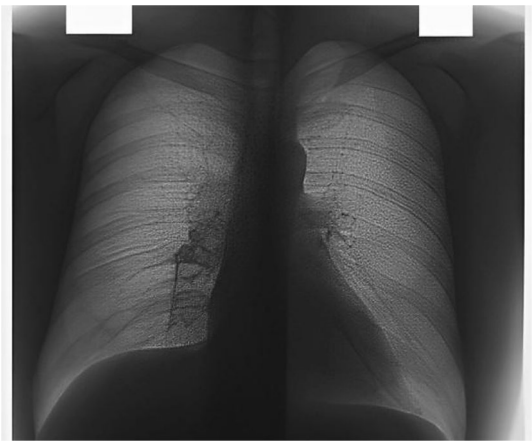

Fig. 14 Input query image DWT LL quantities

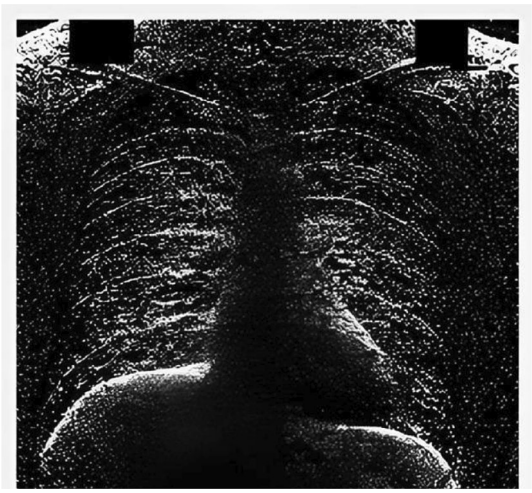

Fig. 15 Input query image DWT LH quantities

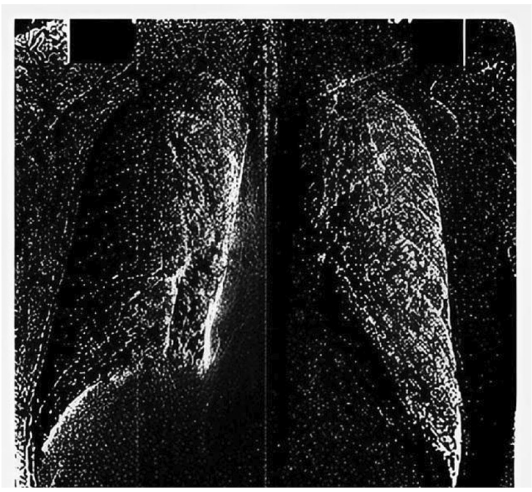

Fig. 16 Input query image DWT HL quantities

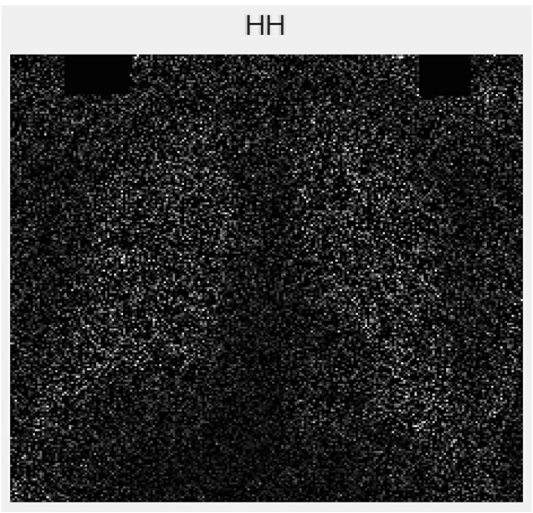

Fig. 17 Input query image DWT HH quantities

In the context of query processing, a particular emphasis is placed on the LL sub-band of the query image. This strategic focus on the LL sub-band signifies a deliberate prioritization of low-frequency components, ensuring that fundamental and essential aspects of the image are underscored and given prominence in the query analysis. By zeroing in on the LL sub-band, the system effectively concentrates on the primary characteristics that significantly contribute to the overall visual representation of the query image. This nuanced and detailed approach enhances the precision and relevance of the query analysis.

Figures 18 and 19 illustrates the processes of horizontal summation and vertical summation on the query image matrix involve mathematical operations that utilize global variables to facilitate computations. These operations are crucial in the study to derive flat and perpendicular projections using lower coefficients obtained from certain image processing techniques, potentially like Discrete Wavelet Transform (DWT).

The process of horizontal summation involves the addition of values along the rows or horizontally within the query image matrix, utilizing global variables to accumulate these sums. This method is aimed at generating a flat projection, offering a condensed overview of the image's horizontal characteristics. The significance of this flat projection lies in its role in computing edge descriptors. By emphasizing features related to changes in intensity or color along the horizontal axis, the system can extract valuable insights into the image's overall horizontal structure. This flat projection becomes a crucial tool for detailed edge analysis, providing nuanced information about the image's composition. In contrast, vertical summation focuses on adding up values along the columns or vertically within the query image matrix, employing global variables for efficient computations. The

goal here is to create a perpendicular projection, offering a condensed representation of the image's vertical features. This perpendicular projection becomes instrumental in enabling the system to compare and evaluate the similarity between different images based on their perpendicular edge characteristics. This proves particularly valuable in tasks such as image matching and similarity assessments, where capturing vertical features is crucial.

Both these summation processes, addressing both horizontal and vertical directions, play a pivotal role in feature extraction and analysis. The flat projection obtained through horizontal summation contributes to the computation of edge descriptors, while the perpendicular projection derived from vertical summation enables the system to effectively compare and assess the similarity of images based on their vertical edge characteristics. Together, these processes enhance the system's capability to extract meaningful features and conduct thorough analyses for various image processing applications.

In Figs. 20 and 21, the horizontal and vertical projections are visually represented, respectively. These projections are

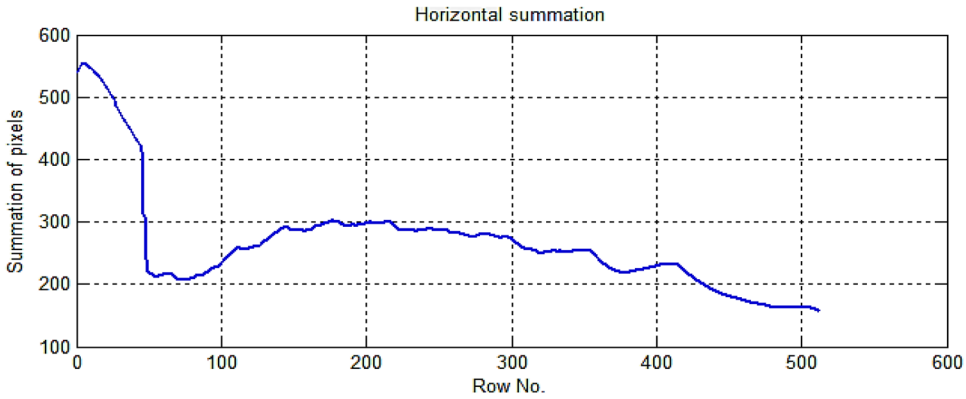

Fig. 18 Input query image flat summation

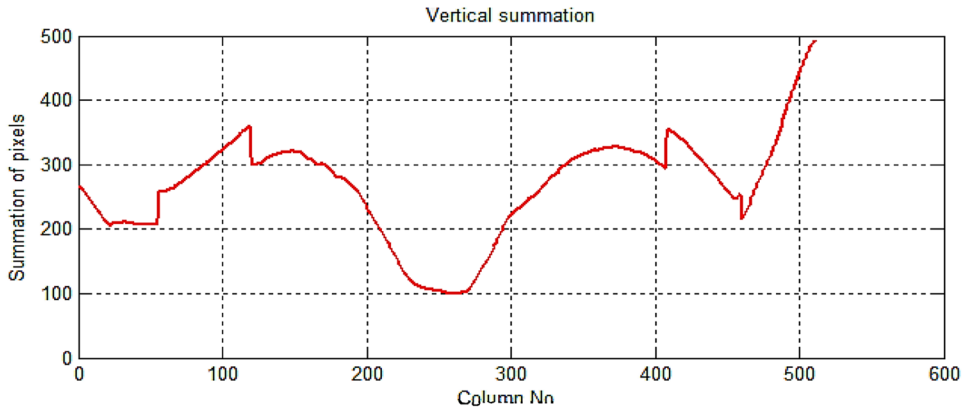

Fig. 19 Input query image perpendicular summation

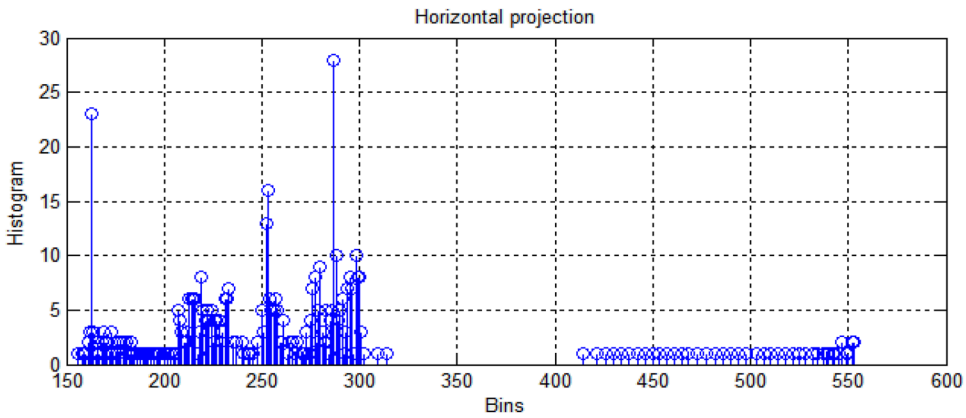

Fig. 20 Input query image flat prognose

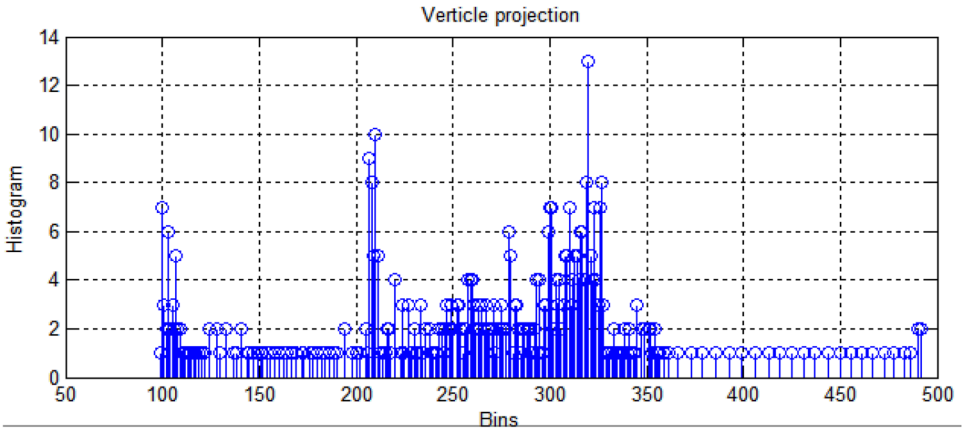

Fig. 21 Input query image perpendicular Prognose

derived by computing histograms of the column-wise sum vectors and row sum vectors of the image.

Figure 20 depicts the horizontal projection obtained by summing the values along each column and constructing a histogram. This projection provides insight into the distribution of features along the horizontal axis of the image. Peaks in the histogram indicate areas with higher intensity or concentration of certain features. The analysis of the horizontal projection aids in understanding the image's characteristics, emphasizing variations and patterns along its width.

Figure 21 conversely depicts the vertical projection generated by summing the values along each row and creating a histogram. This projection offers a view of feature distribution along the vertical axis of the image. Peaks in the histogram highlight regions with distinct characteristics, providing information about variations along the height of the image.

In-depth analysis involves scrutinizing the peaks, valleys, and overall shape of the histograms. Peaks suggest areas of higher feature concentration, while valleys indicate regions with fewer prominent features. The analysis of both projections collectively offers a comprehensive understanding of the image's structural attributes in both the horizontal and vertical directions. This information is valuable for tasks such as pattern recognition, identifying key features, and characterizing the overall composition of the image. By employing histograms of sum vectors, Figs. 20 and 21 provide a visual representation that aids in the nuanced analysis of feature distribution within the image.

Figure 22 provides a detailed insight into the performance of the proposed framework, showcasing an image retrieved from the system. However, the analysis reveals a notable shortfall in the quality of the match within the database. The Bhattacharyya Coefficient, a quantitative measure of similarity, is reported at a low value of 220 for this retrieved image. This low coefficient suggests a substantial divergence in characteristics between the retrieved image and the query image used as a reference.

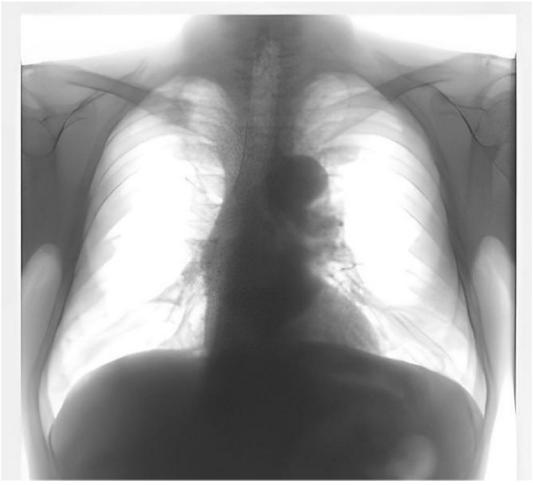

Fig. 22 Database image-11, score = 220

Such in-depth analysis serves as a critical evaluation of the system's effectiveness, highlighting areas where the framework may encounter challenges in accurately retrieving images that closely align with the desired query. Understanding these nuances is essential for refining and optimizing the framework for enhanced image retrieval performance.

Figure 23 portrays the perpendicular prognose projection derived from the row sum vectors of the image. Employing a prognose function on this perpendicular summation vector results in a projection with a relatively low matching score of 220. In the visualization, red bars represent the projection of the query image, while blue bars depict the projection of the database values. The distinct color coding indicates a lower degree of resemblance between them. This suggests that the features captured in the perpendicular direction of the query image do not align closely with those in the database, illustrating a diminished match.

Similarly, Fig. 24 exhibits the flat prognose projection attained by computing column-wise sum vectors of the

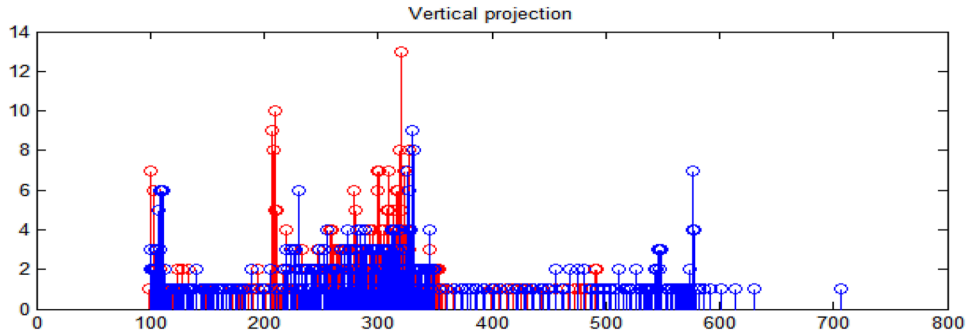

Fig. 23 Perpendicular prognose of database image-11

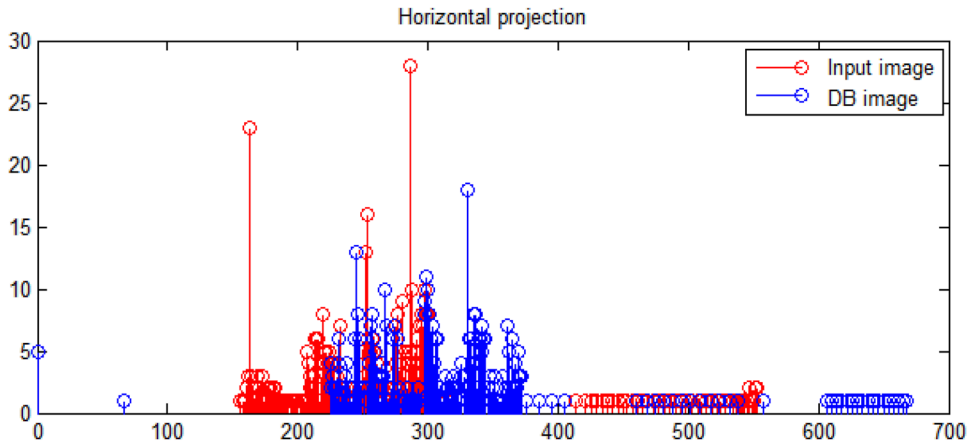

Fig. 24 Flat Prognose of Database image-11

image. The resulting flat prognose projection also yields a low matching score of 220. The red bars signify the projection of the query image, while the blue bars represent the projection of the database values. In this case, larger coefficient values for images in the database indicate a lower degree of resemblance to the query image. The prognose function effectively tallies the measured features, enabling an analysis and visualization of their distribution along the flat axis. This projection captures edge features along the perpendicular direction, offering a visual representation of their distribution. This facilitates an in-depth analysis and examination of the characteristics of these features.

In essence, both projections, whether perpendicular or flat, demonstrate a lower matching score, indicating a limited resemblance between the query image (from Fig. 22) and the images in the database. The tradeoff here lies in the balance between feature distribution and the matching score. While the projections allow for a detailed analysis of feature distribution, the lower matching score implies that the features captured in these projections do not align well with those in the database. This tradeoff underscores the need to carefully consider the nature of features and their distribution in the decision-making process for image matching and retrieval.

Figure 25 displays the top 10 highest matching results from the database, delineated by the Bhattacharyya Coefficient. This coefficient serves as a quantitative measure of similarity between the retrieved images and the query image. Notably, higher coefficient values, such as those presented (351, 349, 342, 339, 337, 335, 332, 329, 326, and 322), signify a more pronounced resemblance, indicating close matches in the characteristic features of the images. The Bhattacharyya Coefficient, in this context, operates as a valuable metric for assessing the likeness between images.

By arranging the coefficient vector in descending order, an efficient retrieval mechanism is established, ensuring that images with the closest matches to the query image's characteristics are prioritized. This sorting process facilitates the identification of images within the database that exhibit the highest similarity to the query image. Consequently, it streamlines the image retrieval process, enabling users to quickly access and retrieve images that share significant similarities with the query image. This approach enhances the effectiveness of image retrieval systems, as it is tailored to prioritize and present the most relevant matches based on their similarities.

In Fig. 26, a graphical representation of the B scores for a collection of images in the database is depicted. The B score serves as a metric quantifying the relationship between the query image and each image in the database. Notably, the plot reveals that approximately eight images exhibit B scores surpassing 300, indicating a notable correlation with

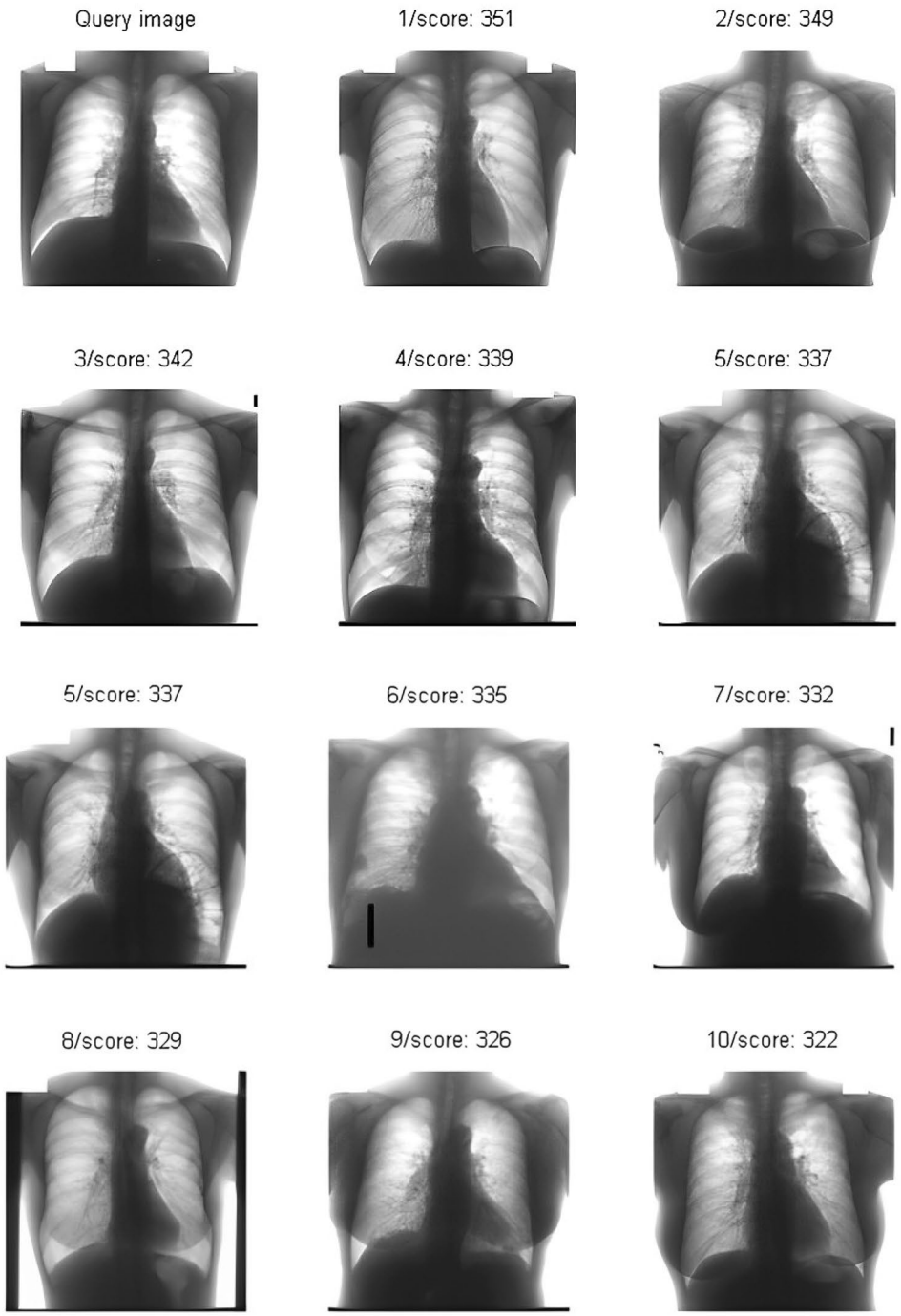

Fig. 25 Database image with top-10 highest scores. Bhattacharyya coefficient = 351

the query image. Among this subset, two images notably approach a B score of 348, denoting a particularly robust resemblance or similarity to the query image.

Conversely, the majority of images in the collection display sub-optimal resemblance to the query image, evidenced by lower B scores. These lower scores suggest a diminished similarity compared to the top matching results. This indicates that a substantial portion of the database images bears weaker resemblance to the query image. The B score plot serves as a valuable tool for assessing the spectrum of similarity between the query image and images in the database. The B score plot provides a comprehensive view of the similarity relationships, with higher B scores indicating stronger matches and lower scores pointing to weaker matches. This graphical representation aids in the efficient identification of images that closely align with the query image, contributing to the nuanced evaluation of image similarities within the database.

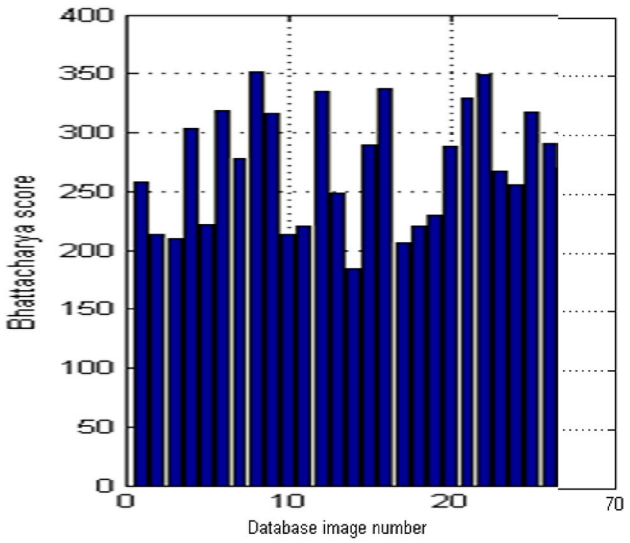

Fig. 26 Bhattacharyya scores vs. database images

Conclusion

A proposed novel method of retrieve a MRI chest image using VBIR technique is inculcating on DT-CWT and EPS filter. Proposed architecture decomposes the Low resolution image using DT-CWT. This method is used since it is shift invariant as well as directional choosing and generates less artifacts as compared with DWT. The dataset is having 20 images for 26 chest samples for various algorithms are estimated and comparative graphs are plotted individually. EPS or Bilateral filtering is used to conserve the boundaries and removing noise the input image and to further improve the performance of the proposed system in terms of MSE, PSNR, RMSE, Entropy and SSIM measurements. Model results highlight the greater enactment of projected technique. DT-CWT also provides the reasonable results. At the clear observation it is illustrated that DT-CWT and EPS filter suited for the Resolution Enhancement of query chest image sample well utilized to get better retrieval rate. This kind of transformed wavelet will putrefies the input signal into 4 diverse components like HH, HL, LH and LL. The B-coefficient is useful to find the accurate reclamation image for a given query image. Then, the similarity score will gives the best image matched with the query image. The database will be training to extract the article of the entire image and then established on this features, the query image will be retrieved. Then, finally based on the similarity score, then system can recuperate the image.

Funding Open access funding provided by Manipal Academy of Higher Education, Manipal.

Data Availability The sample data set information is included in the article that supports the findings of this research.

Declarations

Conflict of interest Authors do not have any conflict of interest.

References

1. Mezzoudj S, Behloul A, Seghir R, Saadna Y. A parallel content-based image retrieval system using spark and tachyon frameworks. J King Saud Univ Comput Inf Sci. 2021;33(2):141–9. https://doi.org/10.1016/j.jksuci.2019.01.003.
2. Cazzato D, Leo M, Distante C, Voos H. When I look into your eyes: a survey on computer vision contributions for human gaze estimation and tracking. Sensors. 2020;20:3739. https://doi.org/10.3390/s20133739.
3. Cedillo-Hernandez M, Garcia-Ugalde FJ, Cedillo-Hernandez A, Nakano-Miyatake M, Perez-Meana H. Visual based video retrieval system for Mexican culture heritage based on object matching and local-global descriptors. In: Mechatronics, electronics and automotive engineering (ICMEAE), 2014 international conference on, Cuernavaca, 2014, pp. 38–43.
4. Aboelenin NA, Elserafi A, Zaki N, et al. Assessment of artificial intelligence-aided computed tomography in lung cancer screening. Egypt J Radiol Nucl Med. 2023;54:74. https://doi.org/10.1186/s43055-023-01014-z.
5. Li Z, Wei C, Li Y, Sun T. Research of shoeprint image stream retrieval algorithm with scale-invariance feature transform. In: Multimedia technology (ICMT), 2011 international conference on, Hangzhou, 2011, pp. 5488–5491.
6. Mohanapriya S, Vadivel M. Automatic retrieval of MRI brain image using multiqueries system. In: Information communication and embedded systems (ICICES), 2013 international conference on, Chennai, 2013, pp. 1099–1103.
7. Ghosh S, Ghosh A. Visual based retrieval of malaria positive images from a clinical database. In: Image information processing (ICIIP), 2013 IEEE second international conference on, Shimla, 2013, pp. 313–318.
8. Gygli M, Grabner H, Riemenschneider H, Nater F, Gool LV. The interestingness of images. In: 2013 IEEE international conference on computer vision, Sydney, VIC, 2013, pp. 1633–1640.
9. SenGupta A, Thounaojam DM, Singh KM, Roy S. Video shot boundary detection: a review. In: Electrical, computer and communication technologies (ICECCT), 2015 IEEE international conference on, Coimbatore, 2015, pp. 1–6.
10. Ding Y, Zhao B, You Q, Chai G. Object retrieval based on visual word pairs. In: 2012 19th IEEE international conference on image processing, Orlando, FL, 2012, pp. 1929–1932.

11. Nie T, Huang L, Liu H, Li X, Zhao Y, Yuan H, Song X, He B. Multi-exposure fusion of gray images under low illumination based on low-rank decomposition. Remote Sens. 2021;13:204. https://doi.org/10.3390/rs13020204.
12. de Koning HJ, van der Aalst CM, de Jong PA, Scholten ET, Nackaerts K, Heuvelmans MA, Lammers JJ, Weenink C, Yousaf-Khan U, Horeweg N, van 't Westeinde S, Prokop M, Mali WP, Mohamed Hoesein FAA, van Ooijen PMA, Aerts JGJV, den Bakker MA, Thunnissen E, Verschakelen J, Vliegenthart R, Walter JE, Ten Haaf K, Groen HJM, Oudkerk M. Reduced lung-cancer mortality with volume Ct screening in a randomized trial. N Engl J Med. 2020;382(6):503–13. https://doi.org/10.1056/NEJMoa1911793. (**Epub 2020 Jan 29**).
13. van Riel SJ, Sánchez CI, Bankier AA, Naidich DP, Verschakelen J, Scholten ET, de Jong PA, Jacobs C, van Rikxoort E, Peters-Bax L, Snoeren M, Prokop M, van Ginneken B, Schaefer-Prokop C. Observer variability for classification of pulmonary nodules on low-dose CT images and its effect on nodule management. Radiology. 2015;277(3):863–71. https://doi.org/10.1148/radiol.2015142700. (**Epub 2015 May 22**).
14. Sverzellati N, Silva M, Calareso G, Galeone C, Marchianò A, Sestini S, et al. Low-dose computed tomography for lung cancer screening: comparison of performance between annual and biennial screen. Eur Radiol. 2016;26:3821–9.
15. Travis WD, Brambilla E, Nicholson AG, WHO Panel, et al. The 2015 World Health Organization classification of lung tumors: impact of genetic, clinical and radiologic advances since the 2004 classification. J Thorac Oncol. 2015;10(9):1243–60. https://doi.org/10.1097/JTO.0000000000000630.
16. Dehmeshki J, Amin H, Valdivieso M, Ye X. Segmentation of pulmonary nodules in thoracic CT scans: a region growing approach. IEEE Trans Med Imaging. 2008;27(4):467–80.
17. Chung M, Tam K, Wallace C, Yip R, Yankelevitz DF, Henschke CI, I-ELCAP Investigators. International early lung cancer action program: update on lung cancer screening and the management of CT screen-detected findings. AME Med J. 2017;2:129.
18. McKee BJ, Regis SM, McKee AB, Flacke S, Wald C. Performance of ACR Lung-RADS in a clinical CT lung screening program. J Am Coll Radiol. 2015;12:273–6.